ACS SyntheticBiology
Research Article
Cite This: ACS Synth. Biol. 2019, 8, 119−126
pubs.acs.org/synthbio

Designing Spatially Distributed Gene Regulatory Networks To Elicit Contrasting Patterns

Mika Tei,*[,†,#] Melinda Liu Perkins,[‡,#] Justin Hsia,[‡,∥] Murat Arcak,[‡] and Adam Paul Arkin*[,§,⊥]

[†]The UC Berkeley−UCSF Graduate Program in Bioengineering, University of California − Berkeley, Berkeley, California 94704, United States

[‡]Department of Electrical Engineering and Computer Sciences, University of California − Berkeley, Berkeley, California 94704, United States

[§]Department of Bioengineering, University of California − Berkeley, Berkeley, California 94704, United States

[⊥]Environmental Genomics and Systems Biology Division, Lawrence Berkeley National Lab, Berkeley, California 94720, United States

Supporting Information

ABSTRACT: Pattern formation and differential interactions are important for microbial consortia to divide labor and perform complex functions. To obtain further insight into such interactions, we present a computational method for simulating physically separated microbial colonies, each implementing different gene regulatory networks. We validate our theory by experimentally demonstrating control over gene expression patterns in a diffusion-mediated lateral inhibition circuit. We highlight the importance of spatial arrangement as a control knob for modulating system behavior. Our systematic approach provides a foundation for future applications that require understanding and engineering of multistrain microbial communities for sophisticated, synergistic functions.

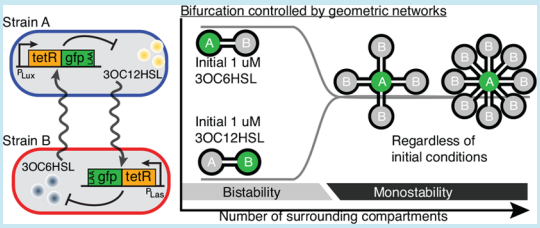

KEYWORDS: *systems biology, synthetic biology, pattern formation, lateral inhibition*

Over the past two decades, synthetic biologists have sought to engineer microbes and their consortia to execute ever more complex tasks. These range from the relatively straightforward production of valuable chemicals[1] to the computation of complex logics[2−4] that allow the microbes to make sophisticated decisions to optimize such production[5−7] or release therapeutics *in situ*.[8,9] There has been sustained interest in both expanding the intrinsic size of these "circuits" for implementation of even more ambitious functions and spreading these circuits among different members of a population that distributes the production load,[10,11] allows reuse of components,[12] or better utilizes space[13−17] and growth.[18−20] Certainly, in nature, microbial populations and consortia spatially arrange themselves to form specialized structures that have mechanical, developmental, and chemical advantages over homogeneous distributions.[21−25]

Ideally, spatial patterning arises in a self-organized fashion from control among individual cells, but shaping communities of cells remains a challenge to engineer.[26] In natural systems, this organization often relies on highly specific communication among cells and/or among highly spatially constrained signaling such as cell contact-mediated mechanisms.[27] In bacteria, intercellular signaling systems like acyl homoserine lactones (AHL) used in quorum-sensing (QS) tend to be fairly nonspecific and long-range, while contact-mediated systems like Cdi-A/B[28,29] are not easily programmable. However, it is possible to experimentally explore the principles of spatial organization among microbial populations by imposing external constraints on communication.

Here, we formulate a simple extensible modeling framework that provides a systematic way to represent the dynamics of multistrain communities, and design a compartmentalized culturing platform to control the spatial arrangement of bacterial colonies harboring different genetic circuits, where the communication between colonies is constrained to specified channels on the device. We demonstrate the utility of the approach by applying the framework to the canonical example of lateral inhibition[30] to predict the emergence of stable contrasting patterns.

RESULTS AND DISCUSSION

Spatial Distribution Introduces a New Control Knob to the Conventional Gene Regulatory Network. To explore the effects of spatial configuration on a gene regulatory network, we propose a structured bacterial communication device consisting of compartments and channels (Figure 1A). Bacterial colonies harboring diffusible signal sensing/producing circuits grow in segregated compartments, and channels establish specific cell−cell communication between the

Received: September 7, 2018
Published: December 12, 2018

DOI: 10.1021/acssynbio.8b00377
ACS Synth. Biol. 2019, 8, 119−126

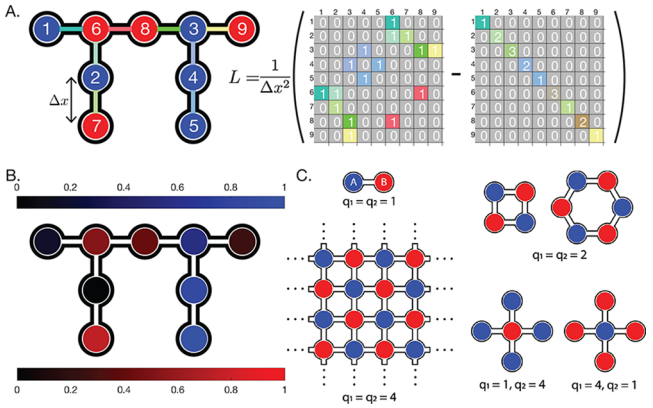

Figure 1. A spatially distributed gene regulatory network established by intercellular communication between bacterial subpopulations separated by compartments. (A) Example of the Laplacian matrix constructed from an arbitrary network. Δx refers to the length of the channels connecting adjacent compartments. (B) Simulated steady-state pattern from the example network when cross-repressive interactions are used between the two cell types. Color represents concentrations of repressor in cell types A and B, normalized to the maximum concentration across all colonies. The parameters are as given in Table S2 where corresponding biochemical parameter values are equal between strains. (C) Examples of reducible spatial configurations. Within each configuration, all channels are the same length and all compartments of the same type are connected to the same number of neighbors. Type A compartments have q_1 neighbors of Type B, and Type B compartments have q_2 neighbors of Type A. Triple dots indicate repetition of the layout into infinity. Configurations such as these can be reduced in dimension when solving for contrasting steady states.

connected colonies. In this section, we develop a mathematical model of this system that permits analyzing dynamic gene regulation distributed across colonies.

A classical intracellular gene regulatory network with two interacting biochemical molecules X and Y can be modeled by

$$\begin{cases} \dfrac{dX}{dt} = -\gamma_X X + f_1(X, Y) \\ \dfrac{dY}{dt} = -\gamma_Y Y + f_2(X, Y) \end{cases} \tag{1}$$

where γ_X, γ_Y are the linear decay rates of X and Y, and functions f_1, f_2 characterize inhibition or activation of a species' production. Adapting this equation to model intercellular communication between compartments introduces spatially descriptive control parameters such as diffusivity, channel length, and the configuration of compartments ("geometry").[31] Cells secrete diffusible molecules that are transmitted along constrained paths to reach other cells, creating biological reaction networks that span multiple cells. For this application, we model colonies of cells whose physical locations are constrained within compartments such that only signaling molecules diffuse through the channels between the compartments. Each compartment is assumed to consist of a single strain that produces only a single species of diffusible molecule, either X or Y. While this work focuses on single-channel communication, the model can also be extended to multi-channel communication, where multiple species of diffusible molecules are present.

In a two-compartment system, we describe the one-dimensional transit of signaling molecules by introducing three new parameters: the channel length l and the diffusivities D_X, D_Y for molecules X and Y, respectively. We approximate the full continuous-space diffusion model by a compartmental model, with the concentration of biochemical species assumed to be constant at all points within the same colony, and assume equal population sizes and exponential growth rates for all colonies (Supplementary Theory Section 1). In doing so, we trade off accuracy in spatial and temporal dynamics for a set of analytically tractable equations that are reasonable when channels are narrow and the volume of compartments and channels is negligible. Then the equations for X and Y produced in separate compartments A and B, respectively, are given by

$$\begin{cases} \dfrac{dX_A}{dt} = -\gamma_X X_A + \dfrac{D_X}{l^2}(X_B - X_A) + f_1(X_A, Y_A) \\ \dfrac{dX_B}{dt} = -\gamma_X X_B + \dfrac{D_X}{l^2}(X_A - X_B) \\ \dfrac{dY_A}{dt} = -\gamma_Y Y_A + \dfrac{D_Y}{l^2}(Y_B - Y_A) \\ \dfrac{dY_B}{dt} = -\gamma_Y Y_B + \dfrac{D_Y}{l^2}(Y_A - Y_B) + f_2(X_B, Y_B) \end{cases} \tag{2}$$

where X_A, Y_A and X_B, Y_B designate the concentrations of X and Y in compartments A and B. Increasing diffusivity or decreasing channel length increases the practical strength and rate of communication between neighboring compartments.

Channeled diffusion permits the design of arbitrary networks whose dimensions increase with each added compartment by the number of biochemical species present within that compartment. To model high-dimensional networks, we use matrices to represent connections between compartments. Given a system with N_A compartments producing X and N_B compartments producing Y, we define the vector $X_A \in \mathbb{R}^{N_A}$ for the concentrations of X in compartments A, and the vector $X_B \in \mathbb{R}^{N_B}$ for the concentrations of X in compartments B. The vectors Y_A and Y_B are defined similarly for molecule Y. We introduce the Laplacian matrix L to represent connections between compartments (Figure 1A). The entries of L are

$$[L]_{ij} = \begin{cases} \dfrac{1}{l_{ij}^2}, \text{ if there is a channel} \\ 0, \text{ if there is no channel} \\ -\displaystyle\sum_{k \neq i} [L]_{ik}, \text{ if } i = j \end{cases}$$

where $l_{ij} = l_{ji}$ is the length of the channel between compartments i and j. The full biochemical dynamics are then described by

DOI: 10.1021/acssynbio.8b00377
ACS Synth. Biol. 2019, 8, 119−126

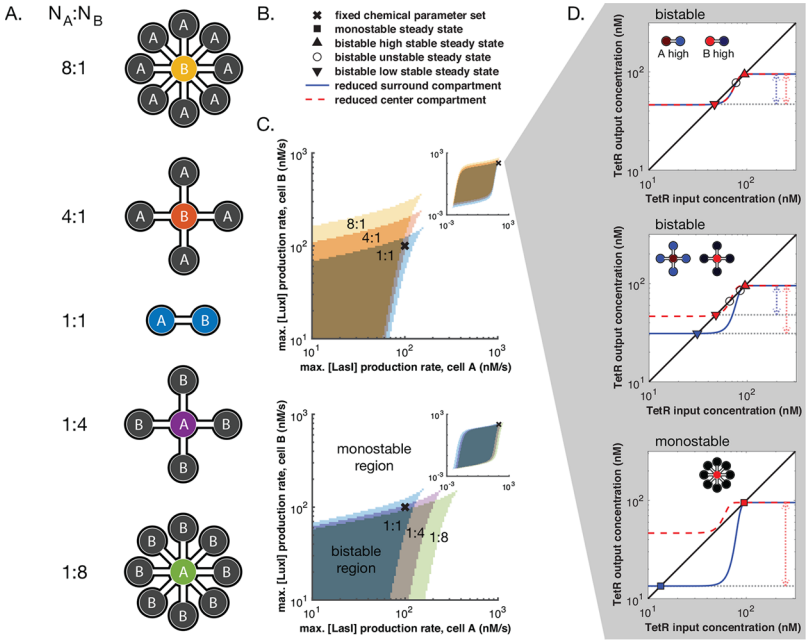

Figure 2. Patterning mechanism and contrast level determined by biochemical parameters and geometries in simulation. (A) Star geometries with varying numbers of surrounding compartments. Throughout the figure, ratios of colony numbers are given as N_A:N_B. (B) Character legend for plots in (C) and (D). (C) Overlaid stability plots show biochemical parameter ranges for which the system is monostable (white) and bistable (shaded, colors corresponding to center compartment of appropriate geometry in (A)). Parameters on the axes are maximum steady-state production rates for LasI (*x*-axis) and LuxI (*y*-axis). Remaining parameters are as given in Table S2 where corresponding biochemical parameter values are equal between strains. As the number of points in the star changes, the shape of the bistable region remains the same (relative to log-scale axes) but shifts relative to the exact biochemical parameter values (insets show the full shape of the bistable region). × indicates an arbitrary set of fixed biochemical parameters that is bistable in the 1:1 and 4:1 cases but monostable for the 8:1 case. (D) For the biochemical parameters indicated by × in (C), a graphical test reveals that contrast may arise from a bistable system (1:1 and 4:1) or from a monostable system with imbalance (8:1) between the input/output characteristics of strains in the reduced systems. Steady states are indicated by ▲ (high expression) and ▼ (low expression) for the bistable case or ■ for the monostable case. In the bistable case with imbalance (4:1), the contrast level (↔) is greater when expression in the center compartment (dashed red) is high than when expression in the surrounding compartments (solid blue) is high. Small insets show corresponding configurations and possible steady-state solutions.

$$\begin{cases} \begin{bmatrix} \frac{dX_A}{dt} \\ \frac{dX_B}{dt} \end{bmatrix} = -\gamma_X \begin{bmatrix} X_A \\ X_B \end{bmatrix} + D_X L \begin{bmatrix} X_A \\ X_B \end{bmatrix} + \begin{bmatrix} f_1(Y_A) \\ 0 \end{bmatrix} \\ \begin{bmatrix} \frac{dY_A}{dt} \\ \frac{dY_B}{dt} \end{bmatrix} = -\gamma_Y \begin{bmatrix} Y_A \\ Y_B \end{bmatrix} + D_Y L \begin{bmatrix} Y_A \\ Y_B \end{bmatrix} + \begin{bmatrix} 0 \\ f_2(X_B) \end{bmatrix} \end{cases} \tag{3}$$

Formulation of the L matrix and the simulated gene expression behavior of an example network are shown in Figure 1A,B.

Dimensionality Reduction Enables Steady-State Analysis of Multicompartmental Cross-Repressive Networks. To apply our mathematical model to a canonical example, we focus subsequent analyses on cross-repression in multicompartmental networks. Lateral inhibition, or mutual inhibition between adjacent units, is a common mechanism to generate contrasting patterns. Here, $f_1(Y)$ and $f_2(X)$ are Hill functions describing repression of the production of the diffusible molecules by the opponent molecules.

Using dimensionality reduction, we can identify the existence of stable contrasting steady-state patterns in systems with a particular class of spatial configurations for which all channels are the same length, all compartments of the same cell type are connected to the same number of other compartments ("neighbors"), and compartments with the same cell type have the same ratio of neighbors belonging to one type *vs* the other type. Arbitrarily large multicompartmental systems with this structure can be reduced in dimension to two-compartmental systems with multiplicative factor adjustments to the diffusion (Figure 1C, Supplementary Theory Section 3). For the remainder of this paper we will consider the special case where compartments of one cell type are connected only to compartments of the other cell type. In particular, if each compartment of type A has q_1 neighbors and each compartment of type B has q_2 neighbors, then the concentrations of repressors in each of the representative compartments *A*, *B* evolve as eq 2 with $D_{X/Y}$ replaced by $q_1 D_{X/Y}$ in *A* (for X_A and Y_A) and by $q_2 D_{X/Y}$ in *B* (for X_B and Y_B). These adjustments corroborate the intuition that a compartment with more neighbors experiences higher diffusive in- and out-flux of the signaling molecules. We use "diffusion-mediated lateral inhibition" (DLI) to refer to multicompartmental cross-repressive networks that satisfy the geometric constraint permitting reducibility. The DLI system is analogous to contact-mediated lateral inhibition mechanisms such as Notch-Delta, with the crucial distinction that DLI acts through diffusion rather than direct contact. Contact-mediated systems can be modeled by replacing the Laplacian matrix with an adjacency matrix weighted by contact area[32] as described in Supplementary Theory Section 3D.

DOI: 10.1021/acssynbio.8b00377
ACS Synth. Biol. 2019, 8, 119−126

The DLI system can be experimentally implemented using two strains of bacteria that communicate *via* orthogonal QS systems[33,34] and internal inverters (repression circuits). One strain of bacteria is seeded in each compartment with connected compartments alternating between strain types. In this implementation, X is the diffusible AHL produced by Strain A and Y is the orthogonal AHL produced by Strain B.

To facilitate the choice of genetic circuit components, we expand eqs 1, 2, 3 to model the dynamics of mRNA

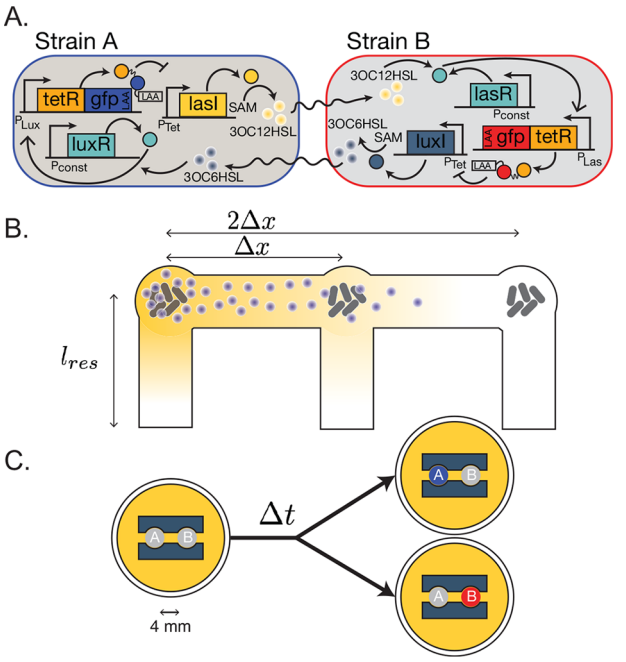

Figure 3. Schematic designs of the DLI system. Arrow-headed lines indicate activation and bar-headed lines indicate inhibition. Throughout the figure, blue represents fluorescence in Strain A and red represents fluorescence in Strain B. (A) Genetic circuit diagram of cross-repressive strains. (B) Channel length Δx is chosen such that AHL diffusion establishes communication between adjacent compartments, but not between nonadjacent compartments with distance $\geq 2\Delta x$. l_{res} defines the efflux channel length that determines the rate of AHL dilution from a compartment to the reservoir. (C) Sketch of DLI device setup. Each compartment of the DLI device is inoculated with one strain type, either A or B. PDMS mold (indigo) is placed on a tissue culture plate to shape solid medium (yellow) into compartments and channels. Contrasting patterns emerge when two strains have different sfGFP-tagged TetR levels in steady state, either high (represented by colored colonies) or low (represented by gray colonies).

transcription/degradation, protein translation/degradation, and AHL synthesis/degradation (Supplementary Theory Section 1). The equilibrium solutions of the augmented model are equivalent to the equilibrium solutions of the original model in eq 3 when f_1 is given by

$$f_1(u) = \frac{\epsilon_{I_A} N_{I_A}}{\gamma_{I_A}} a_1 h_1\left(\frac{\epsilon_{R_A} N_{R_A}}{\gamma_{R_A}} a_2 h_2(u)\right) \tag{4}$$

where h_1 is a Hill function for repressor inhibiting the transcription of AHL synthase and h_2 is a Hill function for AHL activating the transcription of the repressor in the other strain. The Hill coefficients, dissociation constants (K_d), and leakiness of h_1 and h_2 are set by the choice of QS and repressor molecules. Independently, we can change the promoter copy numbers $N_{I_{A/B}}$, $N_{R_{A/B}}$ as well as the translation rates $\epsilon_{I_{A/B}}$, $\epsilon_{R_{A/B}}$ and degradation rates $\gamma_{I_{A/B}}$, $\gamma_{R_{A/B}}$ of AHL synthases and repressors. The composite parameters α_1 and α_2 incorporate the remaining parameters that we cannot easily vary, including maximal transcription rates, mRNA decay rates, and the synthesis rates of AHL by the synthases. The function f_2 is structured similarly except that the order of h_1 and h_2 is reversed (Supplementary Theory Section 1).

Graphical Analysis of a DLI Circuit Predicts Two Mechanisms of Contrasting Pattern Formation. Steady states for the two-compartment diffusion system in eq 2—and hence for the reduced system—can be found graphically by plotting the steady-state output X_A (or Y_B) for constant input X_A (or Y_B) and locating intersections with a line of slope one, since at steady state the output equals the input for the closed-loop system. The graphical test also reveals the stability of the equilibria: one intersection implies the system is monostable while three intersections imply the system is bistable with an unstable homogeneous equilibrium (see Supplementary Theory Section 2).

Contrasting patterns result from disparity in the steady-state target gene expression between cross-repressive strains in a DLI system. Using graphical analysis to assess system equilibria, we construct two-dimensional bifurcation diagrams to reveal two different mechanisms for contrasting pattern generation (Figure 2). One mechanism originates from bistability, in which the system parameters allow two alternative stable states of X and Y production based on initial conditions and possible intrinsic or extrinsic noise/perturbations. The second mechanism occurs in a monostable system when one strain always expresses higher levels than the other.

Ultrasensitivity (cooperativity) in f_1 and f_2 is necessary for bistable contrast. Proper kinetic rate matching ensures that ultrasensitivity is preserved in the feedback loop (Figure S3).[35] In addition to ultrasensitivity, DLI systems must have sufficiently similar inhibition strength between strains to be bistable. When the system loses bistability due to unbalanced inhibition strengths, monostable contrast emerges, with the extent of the contrast depending on the degree of imbalance (Supplementary Theory Section 5B). Changing spatial configuration triggers a bifurcation by modifying the effective inhibition strength between strains (Figure S4).

DLI Network Design and Implementation Require Diffusible Cross-Repression and a Geometric Culturing Platform. Two *Escherichia coli* strains, A and B, were constructed using a pair of orthogonal QS systems[34] and a highly cooperative repressor, *tetR*[36] (Figure 3A). In both strains, *tetR* is translationally fused to the green fluorescent protein reporter, *sfGFP*, with LAA *ssrA* degradation tag in the C-terminus to allow dynamic tracking of the cell state.[37]

The length of the channel (l) between compartments determines the AHL concentration in the neighboring compartments as well as the intercompartmental communication lag time (Figure 3B). A partial differential equation (PDE) model of AHL production, degradation, and diffusion is used to optimize l for sufficient diffusion of AHL to the immediate neighbors while preventing communication between nonadjacent compartments (Figure S5A, Supplementary Theory Section 6). Since AHLs can be stable with a half-life of 6 hour up to days,[38] an efflux channel is added to each compartment to match the dilution rate of AHL to the degradation rates of

DOI: 10.1021/acssynbio.8b00377
ACS Synth. Biol. 2019, 8, 119−126

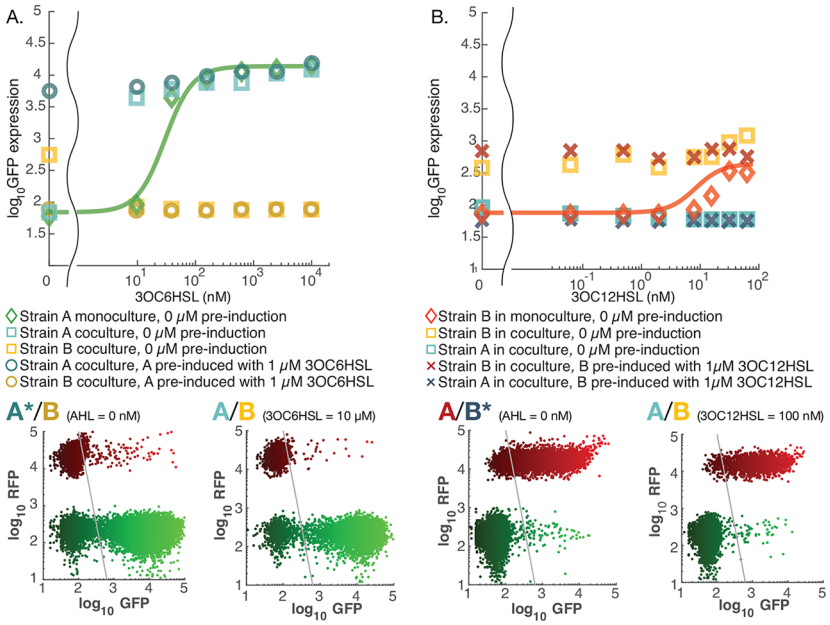

Figure 4. Steady states of the cross-repressive circuit characterized using flow cytometry measurements in liquid cultures. Strain B was identified using constitutively expressed *mRFP1*. Varying concentrations of (A) 3OC6HSL or (B) 3OC12HSL were externally added to the liquid medium (x-axis) and the medians of GFP fluorescence after 8 hour of growth were recorded (y-axis). The markers indicate medians of GFP expression in the corresponding cultures. All of the multistrain cocultures, each represented by □, ○, ×, exhibited contrasting expression profiles between Strains A and B. While the monocultures of Strains A and B showed gently sloped responses to external AHL with Hill function fits of $K_d \simeq 50$ nM and $K_d \simeq 20$ nM (solid lines), the two-strain coculture showed a switch-like response at threshold [3OC6HSL] = 10 nM. Bottom scatter plots show similarity in gene expression patterns between Strain A-biased coculture (A/B 3OC6HSL = 10 μM) and Strain A-preinduced coculture at 8 hour of growth after removing external AHL (A*/B AHL = 0), and Strain B-biased coculture (A/B 3OC12HSL = 100 nM) and Strain B-preinduced coculture at 8 hour of growth after removing external AHL (A/B* AHL = 0).

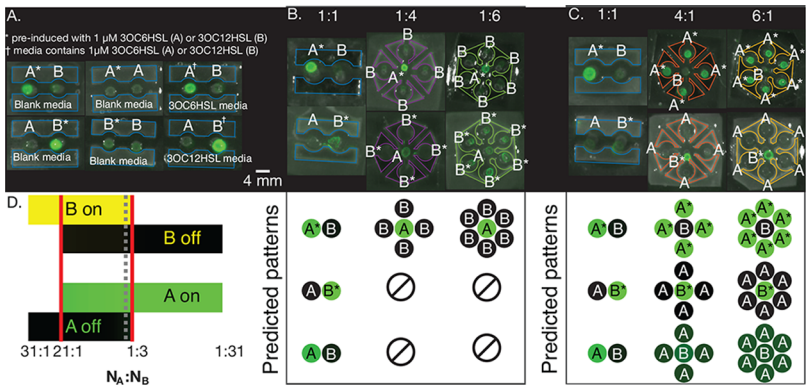

Figure 5. Contrasting pattern formation in various DLI devices. The fluorimeter images were taken after 12 hour of growth at room temperature. * indicates preinduced strains with 1 μM AHL and † indicates strains that were biased to be fluorescent by externally added AHL in medium. (A) 1:1 spatial configuration seeded with cells that had different initial conditions and strain combinations. Devices were seeded with a pair of complementary strains ([A* B], [A B*]), negative controls consisting of a single strain ([A* A], [B* B]), and positive controls of complementary strains where either 1 μM 3OC6HSL or 1 μM 3OC12HSL was mixed in solid medium ([$A^{\dagger}$ B], [A $B^{\dagger}$]). (B,C) 1:1, 1:4, and 1:6 spatial configurations seeded with Strain A at the center surrounded by Strain B (B) or Strain B surrounded by Strain A (C). Top panel shows the fluorimeter images and the bottom panel shows predicted steady-state pattern from computational simulations with the parameter values given in Table S3. When multiple equilibria exist, the predicted patterns are plotted from top to bottom in the order of "A high", "B high", and "unstable". Brighter color indicates higher steady-state reporter expression. (D) Simulated one-dimensional bifurcation diagram in which the ratio of compartments of Strain A:B is used as the bifurcation parameter. The remaining parameters are given in Table S3. Dotted gray line indicates 1:1 spatial configuration. Red solid lines indicate points of bifurcation.

other proteins in the DLI circuit (Figure S5B, Table S3). We use polydimethylsiloxane (PDMS) as the mold to shape solid medium into compartments and channels in specific geometries (Figure 3C, Figure S6).

Bistable and Contrasting Gene Expression Was Observed for DLI Circuit in Liquid Coculture. Before testing pattern formation in compartmental structures, we verified the predicted bistability of the constructed circuits in liquid coculture. Numerical parameters required for the biochemical model eq 4 were determined by experimental measurements of individual modules of AHL reception/activation, transcriptional repression, and AHL synthesis and diffusion in the DLI circuit (Figures S7–S9).

DOI: 10.1021/acssynbio.8b00377
ACS Synth. Biol. 2019, 8, 119–126

Single-cell reporter gene expression was measured using flow cytometry. To examine the existence of two stable steady states, the cocultures were biased with varying external concentrations of 3OC6HSL or 3OC12HSL. While the external AHL inductions in monocultures of Strains A (Figure 4A diamonds and the solid line for the Hill equation fit) and B (Figure 4B diamonds and the solid line for the Hill equation fit) resulted in gently sloped sigmoid responses, the coculture showed a sharp transition in steady state at 10 nM 3OC6HSL (Figure 4 squares), which is a characteristic for a bistable feedback loop.[39]

Another characteristic of bistable systems is hysteresis. To investigate whether our system can reach two heterogeneous steady states in the same culture condition depending on initial conditions, we preconditioned Strains A and B monocultures with the saturated concentration (1 μM) of either 3OC6HSL or 3OC12HSL prior to mixing them into a coculture. The cocultures maintained the distinct gene expression states determined by preconditions over time, while the similarly preinduced monocultures lost the preconditioned state and exhibited sigmoidal induction curves when the cultures were transferred to the fresh media (Figure S10).

The appearance of both the sharp transition and hysteresis confirms that cross-repression between Strains A and B produces an effective intercellular bistable switch.

Bifurcation Is Observed for Cells Grown on the Geometric Culturing Platform. Theoretically, the DLI system with two compartments with proper channel length should behave similarly to the liquid coculture. To investigate bistability and hysteresis in the geometric platform, we preconditioned Strains A and B with either 1 μM 3OC6HSL or 1 μM 3OC12HSL, then washed away the preconditioning media and plated the strains on solid medium before observing their gene expression over time using a plate fluorimeter. The two-compartment geometry plated with complementary strains maintained the preconditioned states over 12 hour whereas the single-strain systems on the same setup quickly lost the preinduced gene expression (Figure 5A). When 3OC6HSL-preinduced Strain A was seeded adjacent to Strain B, Strain A showed high reporter expression while Strain B showed basal expression comparable to the single-strain control, and this difference persisted in time. Similarly, 3OC12HSL-preinduced Strain B seeded adjacent to Strain A showed high reporter expression in Strain B and low reporter expression in Strain A, indicating that contrasting patterns depended on initial conditions.

Next, we evaluated DLI systems in star geometries (Figure 5B,C). We experimentally observed that the system that was bistable in the two-compartments geometry became monostable as the number of outer compartments of Strain B surrounding Strain A increased to four or more (Figure 5B). The monostable contrasting pattern exhibited high reporter fluorescence in the center Strain A regardless of the initial cell states. Strain B, on the other hand, did not shift from monostable to bistable in our experimentally tested geometries, but rather remained bistable with enhanced difference in reporter expression levels as the number of surrounding A increased. Although the experimental setup cannot physically accommodate > 6 compartments, the mathematical simulation suggests that further increasing the number of surrounding compartments would shift the system from bistable to monostable contrast with Strain B expressing high reporter (Figure 5D).

Our results show that we can easily control the geometry of the DLI system to affect circuit behavior and trigger a bifurcation. Geometry may also offset imbalance in biochemical parameters (such as differences in f_1 and f_2 in eq 3, Figure S11) and improve the stability of bistable steady states (Figure 5C).

DISCUSSION

Recent advancement in high-throughput sequencing has revealed that an astonishing range of microbial biodiversity may exist in a single ecosystem.[40] While this paper focuses on spatial interactions between two strains of bacteria with two signaling molecules, the theory may be generalized to handle an arbitrary number of diffusible molecules. A system with m diffusible molecules produced among N total compartments/colonies can be modeled with $m{\cdot}N$ equations, and the number of equations becomes even more if nondiffusible species internal to the compartments must be included in the model. Hence, arbitrary compartmental systems are generally high in dimension and difficult to analyze in full, although symmetries in spatial configuration—such as the alternating-neighbor pattern—may enable mathematical reductions to simplify the search for particular solutions.[41]

For the analyzed DLI system, we explored the role of geometry in determining steady-state behavior. Although we implemented our system with multistrain bacterial colonies, our theory can be applied to isogenic populations as well. Here, the units of interest are individual cells rather than colonies and communication must be contact-mediated since diffusion-based signaling would form self-loops. Dimensionality reduction still applies when cells can be categorized into two separate "classes" by virtue of spatial configuration. Replacing the Laplacian matrix with the adjacency matrix (Supplementary Theory Section 3D) simulates cell-to-cell contact rather than diffusion. The remainder of the analysis then proceeds as before. Extensive and detailed research has been performed to accurately model the developmental processes in metazoans,[32,42,43] and a handful of recent studies have highlighted that spatially relevant parameters such as the number of neighbors or the contact area between them can influence patterning activity even in genetically isogenic cell populations.[44−46] Our work offers a unified interpretation of these results with respect to the imbalance in transfer functions between pairs of representative cells. With sufficient imbalance (Supplementary Theory Section 5B), the system becomes monostable, essentially guaranteeing the fate of the involved cells, and in fact only spatial control knobs can introduce monostable contrast in isogenic populations, since changes to biochemical parameters affect all cells equally. Furthering our understanding of microscale pattern formation would require experimental implementation of controllable contact-based systems. In bacteria, several contact-dependent inhibition systems have been discovered[28,29] for which potential harnessing strategies have been discussed.[47]

Genetic circuit design and implementation are hampered by context-dependent gene expression.[48] Spatial control has advantages over biochemical parameter modification in that it can linearly modulate the effective interaction strength (Figure 5D) *via* the number of connected channels, and the modulation is robust to intracellular conditions. Furthermore, physical separation of the composite strains reduces resource competition among different strains[24] to stabilize the intercellular network. However, spatial control is constrained

DOI: 10.1021/acssynbio.8b00377
ACS Synth. Biol. 2019, 8, 119−126

by structural limitations, such as the maximum number of compartments that fit on the mold or whether the desired communication network can be physically laid out without channels intersecting each other. Thus, synthetic biologists should exploit both biochemical and spatial control knobs for precise design and engineering of microbial consortia.

MATERIALS AND METHODS

Bacterial Strains, Plasmid Construction, and Growth Conditions. *E. coli* strain DH10B (NEB) was used for cloning. PCR amplifications were performed using Phusion High-Fidelity DNA Polymerase (Thermo) and oligonucleotides (IDT). BsaI (NEB) and T7 DNA ligase (NEB) were used to construct plasmids using parts obtained from the MIT Registry of Standard Biological Parts, JBEI registry,[49] or synthesized gBlocks (IDT). RBS calculator[50] was used to generate balanced RBS strengths for *luxI* and *lasI*. TR117 (gift of Thomas L. Ruegg) is a DH10B variant with genomically integrated mRFP1 driven by a constitutive promoter. MOPS EZ Rich Medium (Teknova) and MOPS with 1.5% UltraPure agarose (Thermo) were used for liquid and solid medium. When appropriate, 50 μg/mL Kanamycin or 20 μg/mL Chloramphenicol were added to medium.

Plate Reader Assays. Overnight cultures of cells in MOPS were washed three times and diluted to fresh MOPS at OD600 of 0.3. After 8 hour in 30 °C at 750 rpm, cells were washed three times and diluted to OD600 of 0.025 in a 96 well flat clear bottom black polystyrene microplate (Corning) containing 196 μL MOPS and appropriate concentrations of AHLs (Sigma) dissolved in 4 μL of dimethyl sulfoxide (DMSO) for Figure S7, or 192 μL MOPS and appropriate concentrations of AHLs in 4 μL DMSO and anhydrotetracycline (aTc) (Sigma) in 4 μL ethanol for Figure S8. Synergy 2 (Biotek Instruments) was used to measure cell density (OD600) and fluorescence of growing culture every 8 minute for 12 hour at room temperature. The BioTek excitation and emission wavelengths were 485 nm, 528 ± 20 nm for sfGFP and 560 nm, 620 ± 20 nm for mRFP1.

Flow Cytometry. Overnight cultures of Strains A and B in MOPS were washed three times and diluted to OD600 of 0.03 in fresh MOPS added with 5 ng/mL aTc and 0 or 1 μM AHL for preinduction. After 6 hour of shaking at 750 rpm in 30 °C, cells were washed three times and diluted to OD600 of 0.025 in a 96 well deep well plate (Green BioResearch) containing 196 μL MOPS, 5 ng/mL aTc, and appropriate concentrations of AHLs (Sigma). After 8 hour of shaking at 750 rpm in 30 °C, cells were analyzed using BD LSRFortessa (BD Biosciences). Blue (488 nm) and green (561 nm) lasers were used in combination with 530/30 nm and 610/20 nm filters.

Construction of DLI Device. The compartments and channels in the patterns were cut into 1/8 in. acrylic sheet (McMaster Carr) using a laser cutter (Universal Laser Systems) and then filled with SYLGARD 182 Silicone Elastomer (Dow Corning). PDMS molds were attached to a 6-well clear flat bottom cell culture plate (Falcon), and 3.4 mL of MOPS solid medium was poured into each mold to create DLI devices. aTc in ethanol was added to the final concentration of 5 ng/mL.

DLI Assays. Overnight cultures of Strains A and B in MOPS were washed three times and diluted to OD600 of 0.03 in fresh MOPS added with 5 ng/mL aTc and 0 or 1 μM AHL for preinduction. After 8 hour of shaking at 750 rpm in 30 °C, cells were washed three times and rediluted to OD600 of 2.0 in fresh MOPS. 0.5 μL of the culture was seeded onto each compartment of the DLI device. Gel Doc XR+ System (Biorad) was used to image bacterial colonies every 30 minute for 12 hour in room temperature. The blue epi illumination at 488 nm and 530/28 nm filter was used for sfGFP and the green epi illumination at 532 nm and 605/50 nm filters were used for mRFP1. Camera exposure time of 100 ms was used for all images.

Computational Modeling and Simulation. We used custom code for computational modeling and data analysis in MATLAB (Mathworks). Details about the model construction are provided in Supplementary Theory. Model species and parameters are described in Table S2 and S3.

ASSOCIATED CONTENT

Supporting Information

The Supporting Information is available free of charge on the ACS Publications website at DOI: 10.1021/acssynbio.8b00377.

Supplementary theory, tables, and figures (PDF)

AUTHOR INFORMATION

Corresponding Authors

*E-mail: mtei1@berkeley.edu.
*E-mail: aparkin@lbl.gov.

ORCID

Mika Tei: 0000-0002-8103-3159

Present Address

[‖]Paul G. Allen School of Computer Science and Engineering, University of Washington, Seattle, Washington 98195, United States.

Author Contributions

[#]Mika Tei and Melinda Liu Perkins contributed equally to this work. M.T., M.L.P., J.H., A.P.A., and M.A. designed the research. M.T. and J.H. performed the experiments. M.L.P. and M.T. performed computational modeling. M.T., M.L.P., A.P.A., and M.A. discussed data analysis, and M.T. and M.L.P. performed the analyses. M.T. and M.L.P. wrote the manuscript, and all authors contributed to revising the manuscript.

Notes

The authors declare no competing financial interest.

ACKNOWLEDGMENTS

The authors thank NIH National Institute of General Medical Sciences grant 1R01GM109460-01, Air Force Office of Scientific Research grant FA9550-14-1-0089, and Defense Advanced Research Projects Agency grant BAA-16-17 for support. The DH10B variant TR117 was provided by Dr. Thomas L. Ruegg, and the backbone image processing scripts were provided by Lynn D. Kong. We thank Prof. Michel Maharbiz for comments and discussions, and Prof. Dave Savage for kindly letting us use his plate fluorimeter.

REFERENCES

(1) Hsu, T. M., Welner, D. H., Russ, Z. N., Cervantes, B., Prathuri, R. L., Adams, P. D., and Dueber, J. E. (2018) *Nat. Chem. Biol. 14*, 256−261.
(2) Moon, T. S., Lou, C., Tamsir, A., Stanton, B. C., and Voigt, C. A. (2012) *Nature 491*, 249−253.

DOI: 10.1021/acssynbio.8b00377
ACS Synth. Biol. 2019, 8, 119−126

(3) Nielsen, A. A. K., Der, B. S., Shin, J., Vaidyanathan, P., Paralanov, V., Strychalski, E. A., Ross, D., Densmore, D., and Voigt, C. A. (2016) *Science 352*, 53.
(4) Lee, Y. J., Kim, S.-J., and Moon, T. S. (2018) *ACS Synth. Biol. 7*, 853−865.
(5) Bokinsky, G., Peralta-Yahya, P. P., George, A., Holmes, B. M., Steen, E. J., Dietrich, J., Lee, T. S., Tullman-Ercek, D., Voigt, C. A., Simmons, B. A., and Keasling, J. D. (2011) *Proc. Natl. Acad. Sci. U. S. A. 108*, 19949−54.
(6) Soma, Y., Tsuruno, K., Wada, M., Yokota, A., and Hanai, T. (2014) *Metab. Eng. 23*, 175−184.
(7) Venturelli, O. S., Tei, M., Bauer, S., Chan, L. J. G., Petzold, C. J., and Arkin, A. P. (2017) *Nat. Commun. 8*, 15128.
(8) Anderson, J. C., Clarke, E. J., Arkin, A. P., and Voigt, C. A. (2006) *J. Mol. Biol. 355*, 619−627.
(9) Anderson, J. C., Voigt, C. A., and Arkin, A. P. (2007) *Mol. Syst. Biol. 3*, 133.
(10) Klavins, E. (2014) *Nat. Biotechnol. 32*, 1198−1200.
(11) Tsoi, R., Wu, F., Zhang, C., Bewick, S., Karig, D., and You, L. (2018) *Proc. Natl. Acad. Sci. U. S. A. 115*, 201716888.
(12) Tamsir, A., Tabor, J. J., and Voigt, C. A. (2011) *Nature 469*, 212−215.
(13) Basu, S., Gerchman, Y., Collins, C. H., Arnold, F. H., and Weiss, R. (2005) *Nature 434*, 1130−1134.
(14) Tabor, J. J., Salis, H. M., Simpson, Z. B., Chevalier, A. A., Levskaya, A., Marcotte, E. M., Voigt, C. A., and Ellington, A. D. (2009) *Cell 137*, 1272−1281.
(15) Prindle, A., Samayoa, P., Razinkov, I., Danino, T., Tsimring, L. S., and Hasty, J. (2012) *Nature 481*, 39−44.
(16) Cao, Y., Feng, Y., Ryser, M. D., Zhu, K., Herschlag, G., Cao, C., Marusak, K., Zauscher, S., and You, L. (2017) *Nat. Biotechnol. 35*, 1087−1093.
(17) Fernandez-Rodriguez, J., Moser, F., Song, M., and Voigt, C. A. (2017) *Nat. Chem. Biol. 13*, 706−708.
(18) Payne, S., Li, B., Cao, Y., Schaeffer, D., Ryser, M. D., and You, L. (2013) *Mol. Syst. Biol. 9*, 1−10.
(19) Din, M. O., Danino, T., Prindle, A., Skalak, M., Selimkhanov, J., Allen, K., Julio, E., Atolia, E., Tsimring, L. S., Bhatia, S. N., and Hasty, J. (2016) *Nature 536*, 81.
(20) Kong, W., Meldgin, D. R., Collins, J. J., and Lu, T. (2018) *Nat. Chem. Biol. 14*, 821.
(21) Mobarry, B. K., Wagner, M., Urbain, V., Rittmann, B. E., Stahl, D. a., Mobarry, B. K., Wagner, M., Urbain, V., Rittmann, B. E., and Stahl, D. a. (1996) *Appl. Environ. Microbiol. 62*, 2156−2162.
(22) Fröstl, J. M., and Overmann, J. (1998) *Arch. Microbiol. 169*, 129−135.
(23) Boetius, A., Ravenschlag, K., Schubert, C. J., Rickert, D., Widdel, F., Gieseke, A., Amann, R., Jørgensen, B. B., Witte, U., and Pfannkuche, O. (2000) *Nature 407*, 623−626.
(24) Kim, H. J., Boedicker, J. Q., Choi, J. W., and Ismagilov, R. F. (2008) *Proc. Natl. Acad. Sci. U. S. A. 105*, 18188−18193.
(25) Mousa, W. K., Shearer, C., Limay-Rios, V., Ettinger, C. L., Eisen, J. A., and Raizada, M. N. (2016) *Nat. Microbiol. 1*, 1−12.
(26) Volke, D. C., and Nikel, P. I. (2018) *Adv. Biosyst. 2*, 1800111.
(27) Toda, S., Blauch, L. R., Tang, S. K. Y., Morsut, L., and Lim, W. A. (2018) *Science 361*, 156−162.
(28) Morse, R. P., Nikolakakis, K. C., Willett, J. L. E., Gerrick, E., Low, D. A., Hayes, C. S., and Goulding, C. W. (2012) *Proc. Natl. Acad. Sci. U. S. A. 109*, 21480−21485.
(29) Garcia, E. C., Perault, A. I., Marlatt, S. A., and Cotter, P. A. (2016) *Proc. Natl. Acad. Sci. U. S. A. 113*, 8296−8301.
(30) Collier, J. R., Monk, N. A. M., Maini, P. K., and Lewis, J. H. (1996) *J. Theor. Biol. 183*, 429−446.
(31) Song, H., Payne, S., Gray, M., and You, L. (2009) *Nat. Chem. Biol. 5*, 929−935.
(32) Arcak, M. (2013) *IEEE Trans. Autom. Control 58*, 1250−1262.
(33) Scott, S. R., and Hasty, J. (2016) *ACS Synth. Biol. 5*, 969−977.
(34) Grant, P. K., Dalchau, N., Brown, J. R., Federici, F., Rudge, T. J., Yordanov, B., Patange, O., Phillips, A., and Haseloff, J. (2016) *Mol. Syst. Biol. 12*, 848−849.
(35) Hooshangi, S., Thiberge, S., and Weiss, R. (2005) *Proc. Natl. Acad. Sci. U. S. A. 102*, 3581−3586.
(36) Stanton, B. C., Nielsen, A. A. K., Tamsir, A., Clancy, K., Peterson, T., and Voigt, C. A. (2014) *Nat. Chem. Biol. 10*, 99−105.
(37) Flynn, J. M., Levchenko, I., Seidel, M., Wickner, S. H., Sauer, R. T., and Baker, T. A. (2001) *Proc. Natl. Acad. Sci. U. S. A. 98*, 10584−10589.
(38) Kaufmann, G. F., Sartorio, R., Lee, S.-H., Rogers, C. J., Meijler, M. M., Moss, J. A., Clapham, B., Brogan, A. P., Dickerson, T. J., and Janda, K. D. (2005) *Proc. Natl. Acad. Sci. U. S. A. 102*, 309−314.
(39) Gardner, T. S., Cantor, C. R., and Collins, J. J. (2000) *Nature 403*, 339−342.
(40) Thompson, L. R., et al. (2017) *Nature 551*, 33.
(41) Rufino Ferreira, A. S., and Arcak, M. (2013) *SIAM Journal on Applied Dynamical Systems 12*, 2012−2031.
(42) Amonlirdviman, K., Khare, N. A., Tree, D. R. P., Chen, W.-S., Axelrod, J. D., and Tomlin, C. J. (2005) *Science 307*, 423−426.
(43) Samoilov, M. S., Price, G., and Arkin, A. P. (2006) *Science's STKE 2006*, 1−10.
(44) Lee, S. S. (2016) *J. Theor. Biol. 404*, 51−65.
(45) Guisoni, N., Martinez-Corral, R., Garcia-Ojalvo, J., and de Navascués, J. (2017) *Development 144*, 1177−1186.
(46) Matsuda, M., Koga, M., Woltjen, K., Nishida, E., and Ebisuya, M. (2015) *Nat. Commun. 6*, 1−12.
(47) Chen, D. (2014) *Designing Genetic Circuits for Memory and Communication*, Ph.D. thesis, University of California, Berkeley, CA.
(48) Cardinale, S., Joachimiak, M. P., and Arkin, A. P. (2013) *Cell Rep. 4*, 231−237.
(49) Lee, T., Krupa, R. A., Zhang, F., Hajimorad, M., Holtz, W. J., Prasad, N., Lee, S., and Keasling, J. D. (2011) *J. Biol. Eng. 5*, 12.
(50) Salis, H. M., Mirsky, E. A., and Voigt, C. A. (2009) *Nat. Biotechnol. 27*, 946−950.

DOI: 10.1021/acssynbio.8b00377
ACS Synth. Biol. 2019, 8, 119−126